Angewandte Chemie
Eine Zeitschrift der Gesellschaft Deutscher Chemiker

Supporting Information

Preparative Mass Spectrometry Using a Rotating-Wall Mass Analyzer

*Pei Su, Hang Hu, Daisy Unsihuay, Di Zhang, Tiziano Dainese, Rosa E. Diaz, Jongsu Lee, Don K. Gunaratne, Haiyan Wang, Flavio Maran, Jianguo Mei, and Julia Laskin**

anie_202000065_sm_miscellaneous_information.pdf

Supporting Information

Table of Contents

Section S1. Experimental Procedures **3**
Section S2. An analytical equation for the ion deposition radius **5**
Section S3. Optimization of the distance between the einzel lens and RWMA **8**
Section S4. Calibration of the rotating electric field **9**
Section S5. IonCCD beam profiles of $Au_{144}(SC_4H_9)_{60}^{n+}$ (n=1,2,3) dispersed by the RWMA operating at different frequencies **10**
Section S6. Deposition radius of $Au_{144}(SC_4H_9)_{60}^{n+}$ (n=1,2,3) from SIMION simulations, theoretical calculations and experiments **11**
Section S7. SIMION simulations of the charge state distribution of Apoferritin separated by the RWMA **12**
Section S8. Schematic diagram of the TEM grid holder used for $Au_{144}(SC_4H_9)_{60}$ cluster deposition **13**
Section S9. STEM image of deposited $Au_{144}(SC_4H_9)_{60}^{+}$ on graphene-coated Cu grid **14**
Section S10. HRTEM images of deposited $Au_{144}(SC_4H_9)_{60}^{+}$ on graphene-coated Cu grid. **15**
Section S11. Peak width of the nano-DESI profiles of the PAM individual oligomers **16**
Section S12. ESI-MS spectrum of PDMS oligomers and a list of accurate masses of the oligomers **17**
Section S13. IonCCD beam profile of PDMS oligomers dispersed by the RWMA **18**
References **19**
Author Contributions **20**

SUPPORTING INFORMATION

Experimental Procedures

1. Sample preparation:

$Au_{144}(SC_4H_9)_{60}$ was synthesized according to a known procedure.[1] A solution of $Au_{144}(SC_4H_9)_{60}$ used for soft landing experiments was prepared by dissolving the powder in toluene/methanol=70%/30% to reach a final concentration of 25 µM.

Polyacrylamide (PAM, M_p=2700, M_W=3200, M_n=2500) was kindly provided by Dr. Fan Pu and Prof. R. Graham Cooks (Department of Chemistry, Purdue University). The PAM oligomer solution used for ESI was prepared by dissolving the powder in H_2O/methanol=10%/90% to a final concentration of 100 µM.

Polydimethylsiloxane (PDMS, Mn=~580) was purchased from Sigma-Aldrich (St. Louis, MO). PDMS oligomer solution used for ESI was prepared by dissolving the PDMS in methanol/toluene=70%/30% with 10mM ammounium acetate to a final concentration of 100 µM.

The three organic dyes, 2-[4-(Dimethylamino)styryl]-1-ethylpyridinium (m/z=253.2), Malachite green (m/z=330.2) and Victoria blue B (m/z=470.3) were purchased from Sigma-Aldrich (St. Louis, MO). A solution containing all three dyes at same concentration (45 µM each) for soft landing experiment was prepared by dissolving the dyes in methanol.

2. Generation of the rotating electric field:

The RWMA was powered by eight identical sinusoidal waveforms in the 5-100 kHz frequency range and <10 $V_{0\text{-}p}$ amplitude. The eight waveforms were generated using four dual channel Rigol DG1022Z arbitrary waveform generators (Beaverton, OR).

Synchronization of the function generators produces eight identical waveforms with a 45° phase shift between each waveform. In order to achieve synchronization, the function generators were first connected through the 10MHz in/out using BNC cables. In the next step, one of the function generators was designated as the internal clock, to which the other three units were synchronized. After the frequency and amplitude of each waveform were selected, one of the waveforms was designated as the start phase reference (start phase=0°). The start phases of the rest waveforms were adjusted accordingly (start phase=45°,90°, 135°, 180°,225°, 270°, 315°) by monitoring them on an oscilloscope.

3. Voltages for ion soft landing experiments:

Details of the voltage settings of the high-transmission ESI interface for the ion soft landing experiments are described in our previous publication.[2] Typical RF levels for High-Pressure Funnel (HPF), Low-Pressure Funnel (LPF) and Bent Flatapole are ~270 V, ~135 V and ~400 V, respectively. Typical DC settings for positive and negative ions are: 376/-385 V (Inlet), 384/-400 V (HPF Repeller In), 333/-355 V (HPF Repeller Out), 332/-354 V (HPF Funnel In), 164/-150 V (HPF Funnel Out), 163/-149 V (LPF Funnel In), 28/-28 V (LPF Lens), 32/-32 V (LPF Funnel Out), respectively. We note that the resonance frequency of the bent flatapole ion guide was reduced to 1.17 MHz to improve the transmission of high-*m/z* ions.[3] Typical voltages on the einzel lens are 23/2/23 V and -17/3/-17 V for positive and negative ions, respectively.

4. SIMION simulations:

Ion trajectories were simulated using SIMION 8.0 software package (Scientific Instrument Services, Ringoes, NJ). The geometry of the electrodes were generated using a Lua macro. The resolution of the geometry was defined as 0.3175 mm per grid unit. In the simulation, typical ion beam produced from the source had a FWHM of 0.5 mm. 5000 ions of the same m/z and kinetic energy were produced with a birth step of 0.02 µs to generate a ring-shaped pattern on the collector plate.

5. Surface preparation and characterizations:

1H,1H,2H,2H-perfluorodecanethiol (FSAM, $CF_3(CF2)_7CH_2CH_2SH$) was purchased from Sigma-Aldrich (St. Louis, MO). An FSAM on a gold surface was prepared as follows: a 50 × 15 mm gold coated silicon wafer (100 nm Au layer and 5 nm Cr adhesion layer, Structure Probe Inc., West Chester, PA, USA) was ultrasonically washed in methanol, cleaned by a UV Ozone cleaner (Novascan Technologies Inc., Boone, IA, USA) and immersed in 15 mM solution of FSAM in methanol in a glass petri dish. The monolayer was allowed to assemble for at least 12 h and then ultrasonically washed for 5 min in methanol. The surface was subsequently rinsed with methanol, dried under nitrogen before used for the soft landing experiments. A clean bare gold surface for PDMS deposition was prepared by ultrasonication in methanol followed by cleaning by a UV ozone cleaner.

Direct infusion ESI-MS of PAM and PDMS oligomers and nano-DESI experiments were performed on an Agilent 6560 IM Q-TOF mass spectrometer (Santa Clara, CA, USA). 9:1 methanol:water (v/v) was used as the extraction solvent for the nano-DESI experiments. The nano-DESI probe was assembled by forming a liquid bridge between the primary and nanospray fused silica capillaries (OD 150 µm x ID 50 µm). The extracted analytes were delivered to the mass spectrometer inlet through the nanospray capillary and ionized by ESI. The surface was mounted on an *xyz* motorized stage (Zaber Technologies Inc., Vancouver, BC, Canada), which was used to perform nano-DESI line scans.

Lacey carbon copper grid coated with CVD graphene film (300 mesh) was purchased from Graphene Laboratories Inc. (Ronkonkoma, NY, USA). TEM and HRTEM experiments were performed using a FEI Themis Z operated at 300 kV acceleration voltage. STEM experiments were performed using a FEI Talos 200X operated at 200 kV.

Contact angle measurements were performed using a Ramé-Hart Model 210 Goniometer/Tensiometer (Ramé-Hart Instrument co, Succasunna, NJ, USA). In these experiments, we placed deionized water droplets (1 µL) onto different locations on

the surface and acquired optical images of the water droplets. The contact angles of the droplets were determined using a DROPimage Pro software (Ramé-Hart Instrument co, Succasunna, NJ, USA) by taking the average of ten times of measurement.

Results and Discussion

Section S2

An analytical equation for predicting the radius of the deposition ring:

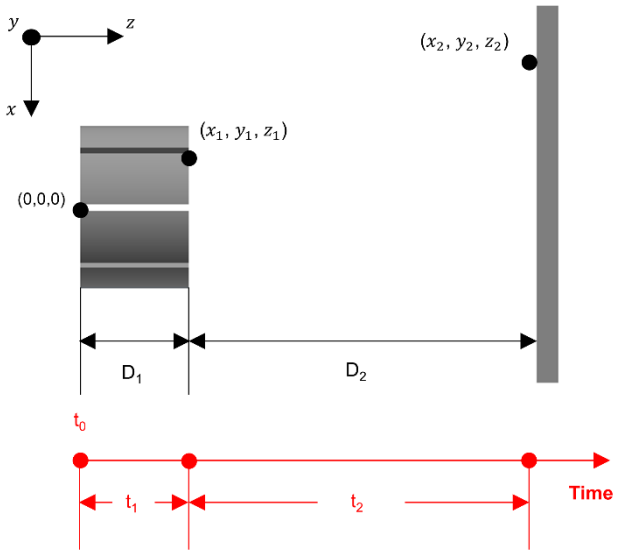

Figure S1. Schematic diagram of the setup for ion dispersion using RWMA in a Cartesian coordinate system.

An ion of mass m, charge z, and kinetic energy per charge of E_K enters the RWMA (operating at a frequency f) at the origin denoted as (0,0,0) at time t_0 and moves along the cylinder's central axis (*z* axis). The ion's travel time through the RWMA is denoted as $t_1 t_1$. During this time, the ion beam is being radially dispersed in the *x*-*y* plane. After exiting the RWMA at a coordinate denoted as (x_1, y_1, z_1), the ion drifts through the field-free region with the velocity vector it attains at the end of the RWMA (v_x, v_y, v_z) and lands onto a grounded target surface at a coordinate denoted as (x_2, y_2, z_2). The travel time in the field-free region is denoted as t_2. The final location of the ion in the x-y plane is determined by the sum of the radial displacement in the RWMA and drift motion in the field-free region (equation 1):

$$x_2 = x_1 + v_x t_2$$
$$y_2 = y_1 + v_y t_2 \quad (1)$$

Previous studies have demonstrated that the rotating electric field is homogeneous in a large area inside the RWMA.[4] We also examined the rotating electric strength using SIMION simulations and constructed a contour plot in the *x*-*y* plane to show the spatial distribution of the field strength (Figure S2):

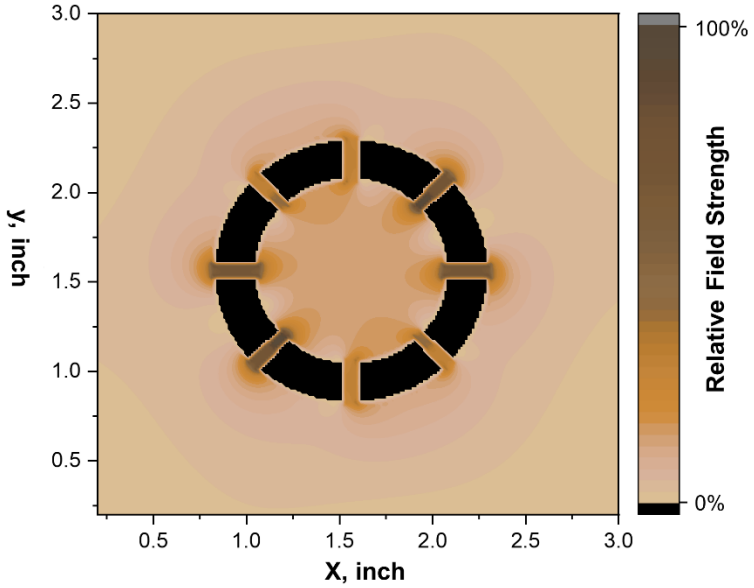

Figure S2. Contour plot of the strength of the rotating electric field in the *x-y* plane. The black region corresponds to the cross section of the RWMA.

Therefore, it is reasonable to assume that the ion experiences the same rotating electric field strength E inside the device when it is dispersed to the off-center locations in the *x-y* plane.
The radial velocity when the ion leaves the RWMA is given by equation 2:

$$\mathrm{v_x(t)} = \int \mathrm{a_x(t)dt} + \mathrm{c_x} = \int \frac{\mathrm{zE}}{\mathrm{m}} \sin \omega \mathrm{t}\, \mathrm{dt} + \mathrm{c_x} = -\frac{\mathrm{zE}}{\mathrm{m\omega}} \cos \omega \mathrm{t} + \mathrm{c_x} \tag{2}$$

Where $\omega = 2\pi \mathrm{f} \omega = 2\pi \mathrm{f}$. Assuming a parallel beam at the origin (i.e. $\mathrm{v_x(t = t_0)} = 0$), we obtain equation 3:

$$\mathrm{c_x} = \frac{\mathrm{zE}}{\mathrm{m\omega}} \cos \omega \mathrm{t_0} \tag{3}$$

Therefore, the velocity components of the ion beam along the x and y axes can be described using equations 4 and 5:

$$\mathrm{v_x(t)} = \frac{\mathrm{zE}}{\mathrm{m\omega}} (\cos \omega \mathrm{t_0} - \cos \omega \mathrm{t}) \tag{4}$$

$$\mathrm{v_y(t)} = \frac{\mathrm{zE}}{\mathrm{m\omega}} (\sin \omega \mathrm{t} - \sin \omega \mathrm{t_0}) \tag{5}$$

The radial displacement inside the RWMA $(\mathrm{x_1}, \mathrm{y_1})$ is given by equations 6 and 7:

$$\mathrm{x_1} = \int \mathrm{v_x(t)dt} + \mathrm{c_x^{'}} = \int (-\frac{\mathrm{zE}}{\mathrm{m\omega}} \cos \omega \mathrm{t} + \mathrm{c_x}) \mathrm{dt} + \mathrm{c_x^{'}} = -\frac{\mathrm{qE}}{\mathrm{m\omega^2}} \sin \omega \mathrm{t} + \frac{\mathrm{qE}}{\mathrm{m\omega}} \mathrm{t} \cos \omega \mathrm{t_0} + \mathrm{c_x^{'}}$$
$$\mathrm{x_1} = (-\frac{\mathrm{qE}}{\mathrm{m\omega^2}} \sin \omega \mathrm{t} + \frac{\mathrm{qE}}{\mathrm{m\omega}} \mathrm{t} \cos \omega \mathrm{t_0} + \mathrm{c_x^{'}}) \Big|_{\mathrm{t_0}}^{\mathrm{t_0+t_1}} = \frac{\mathrm{zE}}{\mathrm{m\omega^2}} (\sin \omega \mathrm{t_0} - \sin(\omega \mathrm{t_0} + \omega \mathrm{t_1}) + \omega \mathrm{t_1} \cos \omega \mathrm{t_0}) \tag{6}$$

$$\mathrm{y_1} = \int \mathrm{v_y(t)dt} + \mathrm{c_y^{'}} = \int (\frac{\mathrm{zE}}{\mathrm{m\omega}} \sin \omega \mathrm{t} + \mathrm{c_y}) \mathrm{dt} + \mathrm{c_y^{'}} = -\frac{\mathrm{qE}}{\mathrm{m\omega^2}} \cos \omega \mathrm{t} - \frac{\mathrm{qE}}{\mathrm{m\omega}} \mathrm{t} \sin \omega \mathrm{t_0} + \mathrm{c_y^{'}}$$
$$\mathrm{y_1} = (-\frac{\mathrm{qE}}{\mathrm{m\omega^2}} \cos \omega \mathrm{t} - \frac{\mathrm{qE}}{\mathrm{m\omega}} \mathrm{t} \sin \omega \mathrm{t_0} + \mathrm{c_y^{'}}) \Big|_{\mathrm{t_0}}^{\mathrm{t_0+t_1}} = \frac{\mathrm{zE}}{\mathrm{m\omega^2}} (\cos \omega \mathrm{t_0} - \cos(\omega \mathrm{t_0} + \omega \mathrm{t_1}) - \omega \mathrm{t_1} \sin \omega \mathrm{t_0}) \tag{7}$$

The landing coordinates of the ion $(\mathrm{x_2}, \mathrm{y_2})$ are given by equations 8 and 9:

$$x_2 = x_1 + t_2 v_x = \frac{zE}{m\omega^2} (\sin \omega t_0 - \sin(\omega t_0 + \omega t_1) + \omega t_1 \cos \omega t_0 + \omega t_2 \cos \omega t_0 - \omega t_2 \cos(\omega t_0 + \omega t_1)) \tag{8}$$

$$y_2 = y_1 + t_2 v_y = \frac{zE}{m\omega^2} (\cos \omega t_0 - \cos(\omega t_0 + \omega t_1) - \omega t_1 \sin \omega t_0 - \omega t_2 \sin \omega t_0 + \omega t_2 \sin(\omega t_0 + \omega t_1)) \tag{9}$$

(9)

The distance of the landing location from the center of the surface (0, 0) is given by equation 10:

$$R = \sqrt{x_2^2 + y_2^2} = \frac{zE}{m\omega^2}\sqrt{2(1 + \omega^2 t_1 t_2 + \omega^2 t_2^2)\left(1 - \cos\omega t_1\right) + \omega t_1(\omega t_1 - 2\sin\omega t_1)}$$

(10)

t_1 and t_2 are not affected by the rotating electric field and are only determined by the initial kinetic energy $\mathrm{E_K}$, the length of the RWMA (D_1) and the drift region (D_2):

$$\mathrm{t}_1 = \mathrm{D}_1\sqrt{\frac{\mathrm{m}}{2\mathrm{E_K}}}$$

$$\mathrm{t}_2 = \mathrm{D}_2\sqrt{\frac{\mathrm{m}}{2\mathrm{E_K}}}$$

(11)

As a result, independent of t_0, the ion is dispersed to a constant distance from the center of the surface. In other words, independent of the starting phase of the rotating electric field, a continuous ion beam of a specific $\mathrm{m/z}$ and $\mathrm{E_K}$ will be dispersed onto a ring with a radius R on the surface.

Section S3

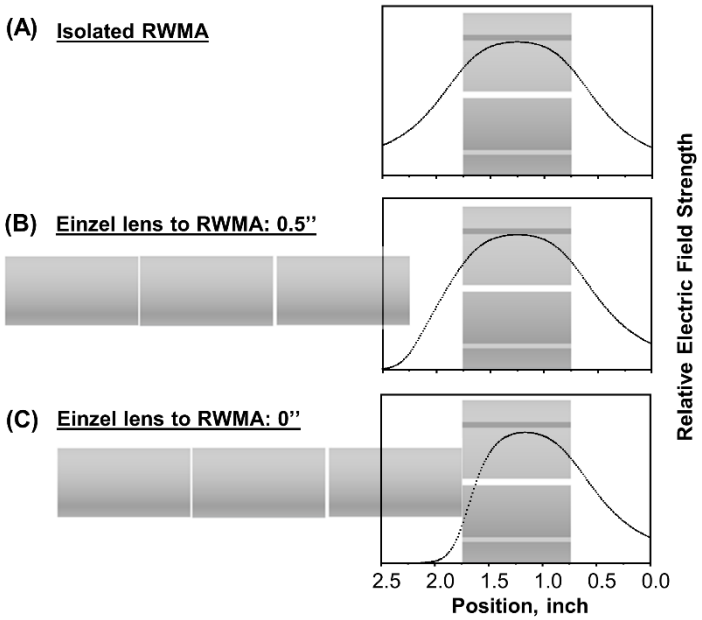

Figure S3. Distribution of the rotating electric field strength along the *z* (instrument) axis in three different scenarios: isolated RWMA A) and RWMA positioned at a distance of 0.5'' B) and 0'' C) from the einzel lens. The first and third element of the einzel lens are set to 0 V.

SUPPORTING INFORMATION

Section S4

Calibration of the rotating electric field:

We observed from SIMION simulations a quadratic decay of the rotating electric field before and after the RWMA (Figure S3). Calibration of the field was carried out in order to obtain an accurate prediction of the deposition radius of the ions using the equation 10. In this experiment, Victoria Blue B (m/z=470.3) was used as a model compound. The deposition radius was measured for different distances between the IonCCD and RWMA (1'', 1.2'', 1.4'', 1.6'', 1.8'', 2'', 2.2'', 2.4'', 2.6'', 2.8'', 3''). The RWMA was operated at f=70 kHz and $V_{0\text{-}p}$=10 V, and the kinetic energy of the ion (E_K) was 35 eV/charge. The experimentally obtained radius at each location was then compared with the corresponding theoretical values, R, and the sum of squares of deviations between the experimental and theoretical values, S, was used to determine the effective strength (E) and length (D_1) of the electric field. Specifically, we used E and D_1 as variable parameters and the GRG nonlinear optimization in Excel Solver to minimize S. The field-free distance (D_2) in equation 10 was adjusted according to D_1. The optimized effective values of E (722 V/m) and D_1 (1.73'') were used for mass calibration throughout the experiments.

Section S5

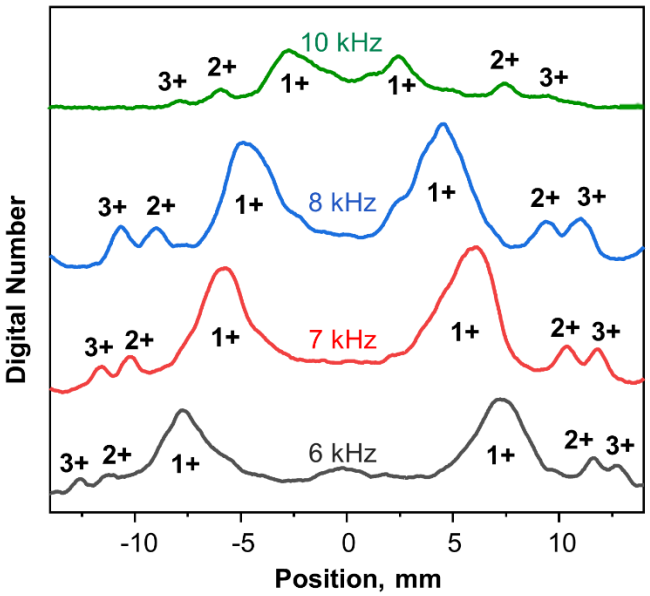

Figure S4. IonCCD beam profiles showing $Au_{144}(SC_4H_9)_{60}^{n+}$ (n=1,2,3) separated by RWMA at f=10 kHz (green), 8 kHz (blue), 7 kHz (red), and 6 kHz (grey). The rf amplitude of the RWMA was $V_{0\text{-}p}$=10 V. The charge states of $Au_{144}(SC_4H_9)_{60}$ are labeled on top of the peaks. As it is shown in this figure, the deposition radius and separation between the different charge states of $Au_{144}(SC_4H_9)_{60}$ can be adjusted by changing the frequency of the rotating electric field. Larger radii are observed at f=6 kHz for all the charge states of the cluster. In contrast, all the rings fold back to the center at f=8 kHz and merge at even higher frequencies. The analytical equation presented in section S2 provides additional insights into the experimentally observed change of the radii. The extent of radial dispersion depends on the time the ion spends in the rotating electric field, which is determined by ion's *m/z* and kinetic energy. In the experiment with $Au_{144}(SC_4H_9)_{60}$, RWMA frequency is selected such that the ions are ejected from the rotating field region within the first rf period. The kinetic energy of $Au_{144}(SC_4H_9)_{60}^{n+}$ (n=1,2,3) is defined by the offset of the flatapole (Figure 1E) and is proportional to the charge state of the cluster. The singly-charged $Au_{144}(SC_4H_9)_{60}^{+}$ cluster has the lowest kinetic energy and therefore, spends the longest time in the rotating electric field. At higher RWMA frequencies, this ion is subjected to an additional radial dispersion from the second rf period. Meanwhile, the 2+ and 3+ charge states leave the rotating field within only one rf period. As a result, the ring of the lower charge state may overlap with the higher charge states. To avoid this overlap, the frequency of the RWMA field is selected such that the entire *m/z* packet leaves the rotating field after the first rf period.

SUPPORTING INFORMATION

Section S6

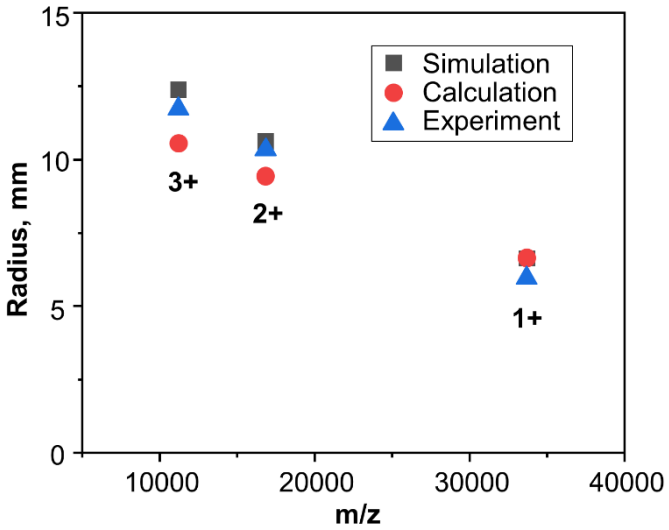

Figure S5. Deposition radius of $Au_{144}(SC_4H_9)_{60}^{n+}$ (n=1,2,3) from SIMION simulations, analytical expression (equation 10), and experiments at f=70 kHz, $V_{0\text{-}p}V_{0\text{-}p}$=10 V with the IonCCD positioned 1'' away from RWMA.

Section S7

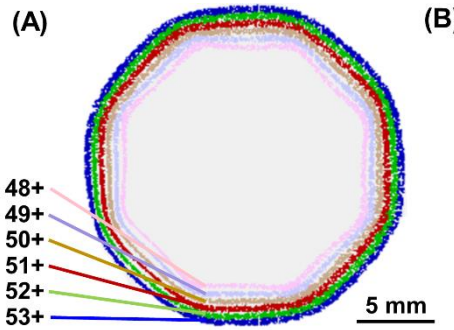

(B)

Charge State	Radius (mm)
48+	10
49+	9.6
50+	9.1
51+	8.7
52+	8.2
53+	7.6

Figure S6. A) SIMION simulations of the native charge state distribution of Apoferritin (480 kDa)[5] separated by RWMA operating at ff =10 kHz, $V_{0\text{-}p}V_{0\text{-}p}$=10 V. The collecting plate is positioned 3'' away from the RWMA. The kinetic energy of the ions is 5 eV/charge. The scale bar in the picture is 5 mm. B) Deposition radius of different charge states of Apoferritin extracted from SIMION simulations presented in A).

Section S8

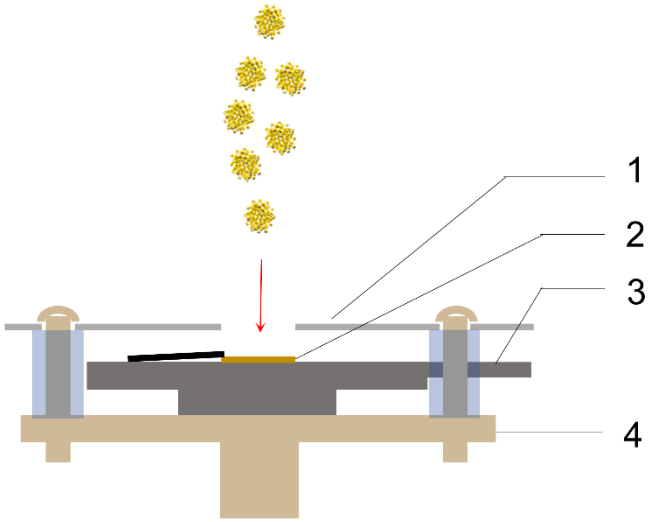

Figure S7. Schematic diagram of the TEM grid holder used for $Au_{144}(SC_4H_9)_{60}$ cluster deposition. 1: grounded mask with a 3 mm diameter aperture in the center; 2: TEM grid; 3: current collector; 4: PEEK adapter connected to a XYZ positioner.

Section S9

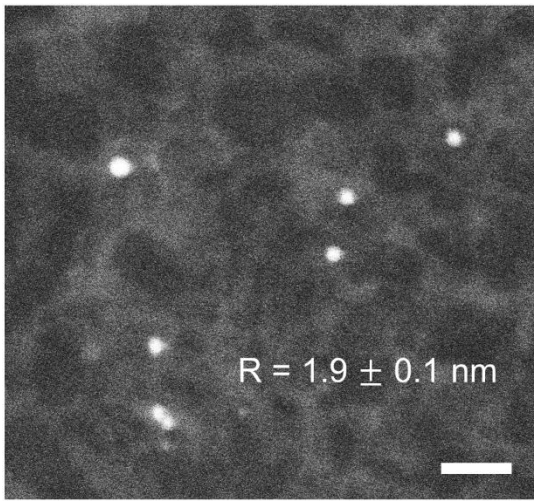

Figure S8. STEM image of deposited $Au_{144}(SC_4H_9)_{60}^{+}$ on graphene-coated Cu grid. The average cluster diameter is labeled. Scale bar: 10 nm.

Section S10

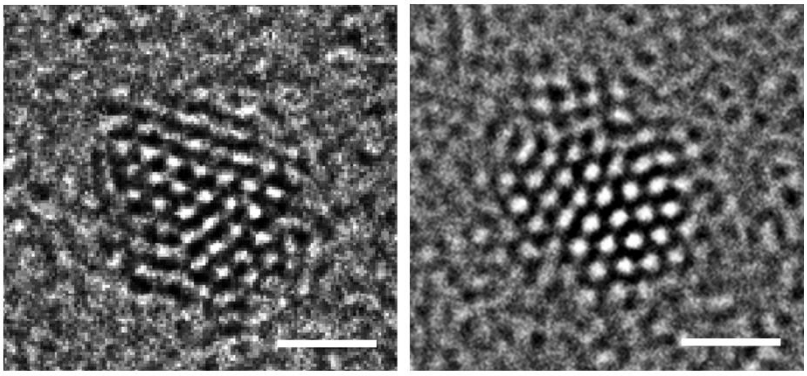

Figure S9. Representative HRTEM images of individual $Au_{144}(SC_4H_9)_{60}^+$ on graphene-coated Cu grid showing fcc-like Au core arrangement. Scale bar=1 nm.

SUPPORTING INFORMATION

Section S11

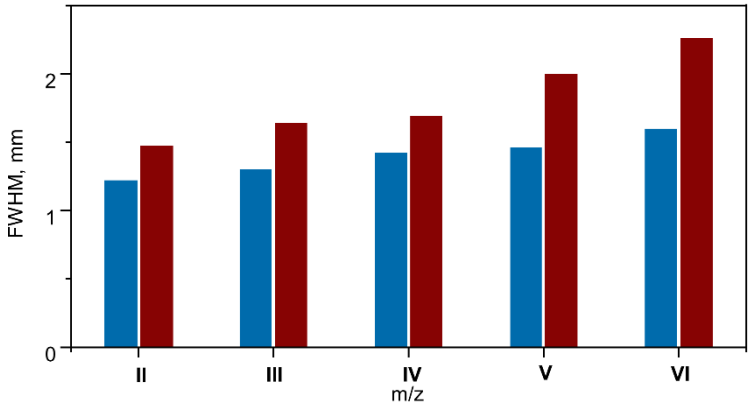

Figure S10. Full-width-at-half-maximum (FWHM) of the nano-DESI profiles of PAM oligomers II through VI on the left side (blue bars) and right side (red bars) of the line scan in Figure 3C.

Section S12

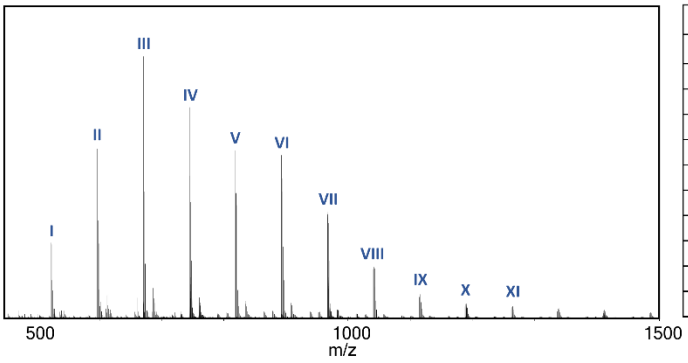

Peaks	m/z
I	552.1861
II	596.2049
III	670.2236
IV	744.2423
V	818.2611
VI	892.2798
VII	966.2989
VIII	1041.3185
IX	1116.3355
X	1190.3541
XI	1264.3728

Figure S11. A positive mode ESI-MS spectrum of PDMS (Mn=~580); *m/z* of the major oligomers observed in the spectrum (I to XI) are listed in the table.

Section S13

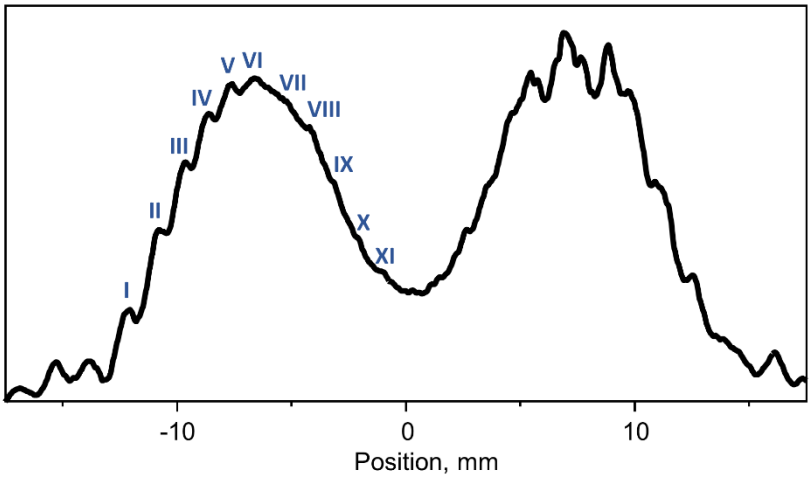

Figure S12. IonCCD beam profile of the PDMS oligomers with RWMA operating at f=50 kHz, V0-p=10 V; peaks corresponding to different oligomers are marked in the figure.

References:

[1] H. Qian, R. Jin, *Chem. Mater*. **2011**, *23*, 2209–2217.
[2] P. Su, H. Hu, J. Warneke, et al., *Anal. Chem.* **2019**, *91*, 5904-5912.
[3] K. L. Fort, M. Van de Waterbeemd, D. Boll, et al., *Analyst* **2018**, *143*, 100-105.
[4] J. Clemmons, F. Herrero, *Rev. Sci. Instrum.* **1998**, *69*, 2285-2291.
[5] A. C. Leney, A. J. Heck, *J. Am. Soc. Mass. Spectrom.* **2017**, *28*, 5-13.

SUPPORTING INFORMATION

Author Contributions

P.S.: Designed and performed the experiments and simulations, analyzed the data, and co-wrote the manuscript. H.H.: Performed the experiments and simulations, assisted with data analysis and interpretation. D.U.: Performed the nano-DESI experiments, assisted with data analysis and interpretation. D.Z.: Performed the TEM and STEM experiments, assisted with data analysis and interpretation. T.D.: Synthesized the Au_{144} clusters. R.E.D.: Performed TEM and HRTEM experiments, assisted with data analysis and interpretation. J.L.: Performed the contact angle measurements. D.K.G.: performed the initial simulations and designed the RWMA device. F.M.: Led the synthesis of the Au_{144} clusters and co-wrote the manuscript. H.W.: Led the TEM and STEM experiments. J.M.: Led the contact angle measurements. J.L.: Led the project, conceived the idea, designed the experiments, and co-wrote the manuscript.